DOI: 10.1021/cg9012735

CRYSTAL GROWTH & DESIGN Article

2010, Vol. 10 1247–1256

Steric Control over Supramolecular Polymer Formation in *trans*-1,2-Bis(4-pyridyl)ethylene Adducts of Zinc Xanthates: Implications for Luminescence

Jun-Gill Kang,*[,†] Jung-Sik Shin,[†] Dong-Hee Cho,[†] Yong-Kwang Jeong,[†] Changmoon Park,[†] Shu Fang Soh,[‡] Chian Sing Lai,[§] and Edward R. T. Tiekink*[,#,⊥]

[†]*Department of Chemistry, Chungnam National University, Yuseong, Daejon 305-764, Republic of Korea,* [‡]*Department of Chemistry, National University of Singapore, Singapore 117543,* [§]*Health Sciences Authority, Outram Road, Singapore 169078,* [#]*School of Materials Science and Engineering, Nanyang Technological University, Singapore 639798, and* [⊥]*Department of Chemistry, University of Malaya, 50603 Kuala Lumpur, Malaysia*

Received October 14, 2009; Revised Manuscript Received November 27, 2009

ABSTRACT: Steric control over supramolecular aggregation is demonstrated for a series of adducts formed between $Zn(S_2COR)_2$ and *trans*-1,2-bis(4-pyridyl)ethylene, whereby supramolecular zigzag polymers are found when R is small, that is, Et (**1**) and *n*-Bu (**2**), but only bimetallic aggregates could be formed when R = Cy (**3**). This results in different coordination geometries: four-coordinate N_2S_2 zinc in **1** and **2**, and five-coordinate NS_4 zinc in **3**, a feature which greatly influences photophysical responses in the solid state. When excited in the UV region, $\{Zn(S_2COEt)_2L\}_\infty$ (**1**) and $\{[Zn(S_2COCy)_2]_2L\}$ (**3**) produce broad luminescence in the visible region. Five-coordinate **3** produces more broad and intense luminescence than four-coordinate **1**. The configuration interaction singles (CIS) and post-Hartree−Fock (HF) calculations for **1** and **3** indicate the A-band excited state is responsible for the observed luminescence which is strongly associated with charge transfer from S and Zn.

Introduction

It is now well established that the generation of coordination polymers holds great potential for new molecular materials with applications in fields as diverse as electronic devices, magnetic materials, separation science, gas storage, and catalysis. In this context, photoluminescence, in particular the generation of blue-emitting materials, is a primary motivation for the investigation of mono-, di-, tetra-, and polynuclear zinc complexes,[1] an endeavor that continues to attract significant attention.[2] This study investigates some of the principles that control molecular aggregation patterns in such compounds and the influence of the resulting structures upon solid-state luminescence.

A crystal engineering design strategy for the control of supramolecular aggregation in several series of zinc-triad dithiolate compounds has emerged from systematic structural investigations,[3] and building upon complementary studies of other main group element systems.[4] For example, it was demonstrated that the systematic variation in steric bulk of the remote R group in compounds of the general formula $Zn(S_2COR)_2$ allowed for the generation of isolated tetranuclear species, featuring 16-membered rings, when R was relatively large, that is, i-propyl. As the steric bulk of R was reduced from *i*-propyl to *n*-propyl, the 16-membered rings were retained but were now connected, via corner-sharing, into a linear chain. Finally, further reduction in the size of R, to ethyl, allowed for the formation of 2-D structures, comprising interconnected, edge-shared, 16-membered rings.[3a] This principle of steric control over supramolecular aggregation has been extended to include other zinc-triad dithiolates,[3] including those containing the dithiophosphate ligand, that is, $^-S_2P(OR)_2$, for R = *i*-Pr and Cy.[3e] Here, it proved possible to control polymer formation (i.e., R = *i*-Pr vs Cy) and topology (e.g., zigzag vs helical) in Lewis base adducts formed between $Zn[S_2P(OR)_2]_2$ and various bipyridine Lewis bases (e.g., 2,2′-dithiopyridine and 1,2-bis(4-pyridyl)propane).[3e] In the dithiophosphate and dithiocarbamate ($^-S_2CNR_2$) systems, there are two R substituents that can contribute to a putative steric effect. The related adduct chemistry with xanthates, with only one R substituent per thiolate ligand, remains relatively unexplored except for a small number of structures, more often than not with chelating bipyridine Lewis bases.[5] Accordingly, a systematic investigation was undertaken in the present study where various adducts of $Zn(S_2COR)_2$, for R = Et, *n*-Bu, and Cy, with *trans*-1,2-bis(4-pyridyl)ethylene were examined. Further, the photoluminescence (PL) properties of these species were studied.

Zinc(II) compounds with chromic ligands have been observed to produce two kinds of luminescence ascribed to $\pi^*-\pi$ intra- or interligand charge transfer processes. The luminescence of pyridyl,[6] benziimidazole,[7] benzothiazol,[8] benzenecarboxamide,[9] biimidazole,[10] and salicylideneamine,[11] each known to emit blue luminescence, is markedly enhanced and red-shifted by complexation to zinc(II). The enhanced intensity of the $\pi^*-\pi$ intraligand luminescence was attributed to an increase in the rigidity of the ligand in the complex compared with the free ligand, resulting in a reduction of nonradiative transition processes. The red-shift of the $\pi^*-\pi$ intraligand luminescence was due to the extension of the π-conjugation by the complexation with zinc(II). By contrast, complexation with Cd(II), Mn(II), Ni(II), Co(II), and Hg(II) quenched the intensity of the $\pi^*-\pi$ intraligand luminescence. The luminescence associated with the ligand-to-ligand charge transfer (LLCT) has been observed for zinc(II) compounds with mixed benzothio (SR) and phenanthroline (phen) ligands.[12,13] For these systems, strong ^{3}LLCT phosphorescence was produced

*Corresponding authors. E-mail: jgkang@cnu.ac.kr (J.-G.K.); Edward.Tiekink@gmail.com (E.R.T.T.).

Published on Web 12/16/2009

Table 1. Crystallographic Parameters and Refinement Details for 1, 2, and 3.2CHCl$_3$

	1	2	3.2CHCl$_3$
formula	$C_{18}H_{20}N_2O_2S_4Zn$	$C_{22}H_{28}N_2O_2S_4Zn$	$C_{40}H_{54}N_2O_4S_8Zn_2\cdot 2CHCl_3$
fw	489.97	546.07	1252.80
temp, K	183	183	223
crystal system	monoclinic	monoclinic	triclinic
space group	$C2/c$	$C2/c$	$P\bar{1}$
a, Å	21.020(3)	16.6563(15)	9.6565(16)
b, Å	6.5819(9)	9.6575(8)	11.2992(18)
c, Å	17.413(2)	16.2426(14)	13.812(2)
α, deg	90	90	105.492(4)
β, deg	120.462(3)	95.210(2)	104.151(4)
γ, deg	90	90	95.771(4)
V, Å^3	2076.6(5)	2602.0(4)	1385.9(4)
Z	4	4	1
μ, cm^{-1}	1.601	1.286	1.496
D_x, g cm^{-3}	1.567	1.394	1.501
no. unique reflns	3035	3809	7903
no. obs reflns with $I > 2\sigma(I)$	2174	3074	3619
R (obs data)	0.043	0.045	0.062
a, b in weighting scheme	0.046, 0	0.051, 0.397	0.041, 0
R_w (all data)	0.100	0.104	0.156
CCDC no.	749885	749886	749887

from phenanthroline (phen) via a pπ(SR) → π^*(phen) transition. Previously,[14,15] it was demonstrated that some gold(I) thiolate complexes produced characteristic luminescence via ligand-to-metal charge-transfer transitions (LMCT). Although extensive studies of the photophysical properties of zinc(II) compounds with thiolate derivatives have been performed,[1,2] optical processes associated with LMCT or MLCT have yet to be reported. In the present investigation, the optical properties of the engineered ternary zinc(II)/xanthate/*trans*-1,2-bis(4-pyridyl)ethylene compounds are investigated. Reflectance, photoluminescence (PL), and excitation spectra of these zinc(II) compounds, *trans*-1,2-bis(4-pyridyl)ethylene and the potassium xanthates were measured. In addition, configuration interaction singles (CIS) and post-Hartree−Fock (HF) calculations on the molecular orbitals and excited states of the complexes were performed to reveal the nature of the absorbing and emitting states.

Experimental Section

Synthesis, General Methods, and Characterization. The Zn(S$_2$COR)$_2$, R = Et, *n*-Bu, and Cy, compounds were prepared in high yields from the reaction of Zn(NO$_3$)$_2\cdot$6H$_2$O (Merck) and the respective potassium xanthate in aqueous solution following the standard procedure.[16] The adducts were obtained from refluxing (2 h) the zinc xanthate (0.2 g) with either a 1 or 2 stoichiometric amount of *trans*-1,2-bis(4-pyridyl)ethylene (L; Aldrich) in CHCl$_3$ solution. After reaction, the solvent was removed in vacuo and the residue was recrystallized by slow evaporation from a CHCl$_3$/acetonitrile (4:1) mixture in each case. The R = Cy compound was characterized crystallographically as a dichloroform solvate, that is, **3.2CHCl$_3$**, but other analysis were performed on dried samples, that is, on **3**. The [ZnL]$^{2+}$ species, prepared as the [ZnL](NO$_3$)$_2$ salt for spectroscopic characterization, was isolated as its nitrate salt from the reaction of Zn(NO$_3$)$_2\cdot$6H$_2$O (Merck) (1 mmol, 0.2975 g) taken in acetonitrile (50 mL) and L (2 mmol, 0.3757 g) dissolved in CHCl$_3$ (50 mL). The mixture was refluxed at 50 °C for 2 h. The precipitate that formed was washed with a 1:1 solution of acetonitrile/chloroform; found: C, 38.6; H, 2.7; O, 25.8; N, 14.4%; and calculated for [ZnL](NO$_3$)$_2$: C, 38.8; H, 2.7; O, 25.8; N, 15.1%.

Infrared data were recorded as KBr discs on a Excalibur Series Bio-Rad Merlin FTS 3000 spectrophotometer. ^{1}H NMR data (CDCl$_3$) were measured on a Bruker ACF 300 MHz FT spectrometer operating at 300.1315 MHz using TMS as the internal reference. Microanalytical data were measured on a Perkin-Elmer PE 2400 CHN Elemental analyzer. Thermogravimetric analyses were performed with a TGA 2050 Thermogravimetric analyzer (TA Instruments) in a nitrogen atmosphere at a heating rate of 20 °C min^{-1}. X-ray powder diffraction patterns were obtained in the 2θ range 10−70° on a Siemens D5005 X-ray diffractometer employing Cu Kα radiation.

{Zn(S$_2$COEt)$_2$L}$_\infty$ (**1**) obs. (calc.): C, 43.96 (44.12); H, 4.24 (4.11%). IR (KBr, cm^{-1}): 1611(s) ν(C=C); 1140(s), 1127(m) ν(C−O); 1027(s) ν(C−S). NMR (CDCl$_3$): ^{1}H δ 8.79 (d, N−C$\underline{H}$, 6.4 Hz), 7.53 (d, N−CHC$\underline{H}$, 6.4 Hz), 7.26 (s, C$\underline{H}$=C), 4.52 (q, C$\underline{H}_2$, 7.2 Hz), 1.45 ppm (t, C$\underline{H}_3$, 7.1 Hz).

{Zn(S$_2$COBu)$_2$L}$_\infty$ (**2**) obs. (calc.): C, 48.13 (48.39); H, 4.92 (5.17%). IR (KBr, cm^{-1}): 1609(s) ν(C=C); 1190(s), 1140(m) ν(C−O); 1050(s) ν(C−S). NMR (CDCl$_3$): ^{1}H δ 8.80 (d, N−C$\underline{H}$, 6.4 Hz), 7.54 (d, N−CHC$\underline{H}$, 6.4 Hz), 7.30 (s, C$\underline{H}$=C), 4.46 (t, OC$\underline{H}_2$, 6.6 Hz), 1.81 (m, OCH$_2$C$\underline{H}_2$, 7.6 Hz), 1.47 (m, C$\underline{H}_2$CH$_3$, 7.6 Hz), 0.97 ppm (t, C$\underline{H}_3$, 7.6 Hz).

{[Zn(S$_2$COCy)$_2$}$_2$L} (**3**) obs. (calc.): C, 45.94 (47.37); H, 5.45 (5.37%). IR (KBr, cm^{-1}): 1609(s) ν(C=C); 1199(s), 1138(m) ν(C−O); 1056(s) ν(C−S). NMR (CDCl$_3$): ^{1}H δ 8.77 (d, N−C$\underline{H}$, 6.0 Hz), 7.51 (d, N−CHC$\underline{H}$, 6.4 Hz), 7.28 (s, C$\underline{H}$=C), 4.52 (m, C$\underline{H}$), 2.07 − 1.25 ppm (m, C$\underline{H}_2$).

Crystallography. Intensity data were measured on a Bruker SMART CCD diffractometer employing Mo Kα radiation to θ_{max} = 30.0°. Data processing and absorption correction were accomplished with SAINT and SADABS, respectively. The structures were solved by heavy-atom methods and refinement (anisotropic displacement parameters, hydrogen atoms in the riding model approximation and a weighting scheme of the form $w = 1/[\sigma^2(F_o^2) + aP^2 + bP]$ for $P = (F_o^2 + 2F_c^2)/3$) was on F^2.[17d] Crystallographic data and final refinement details are given in Table 1. All crystallographic figures were drawn with the DIAMOND program, with the probability ellipsoids of 70% for Figures 1 and 2, and 50% for Figure 4.

Photophysical Studies. For the measurement of reflectance spectra, samples were prepared by pulverizing a small amount (5−10 wt %) with BaSO$_4$. The reflectance spectra of the diluted samples were recorded on an UV-3101PC (Shimadzu) spectrophotometer equipped with an integrating sphere attachment. For PL and excitation spectra measurements, samples in microcrystalline states were placed on the coldfinger of a CTI-cryogenics refrigerator (Helix Tech.) using silicon grease. Excited light from an Oriel 1000-W Xe arc lamp, passed through an Oriel MS257 monochromator, was focused on the sample. The spectra were measured at a 90° angle with an ARC 0.5 m Czerny-Turner monochromator equipped with a cooled Hamamatsu R-933-14 photomultiplier tube. PL spectra were measured with a He−Cd 325-nm laser line.

Results and Discussion

Supramolecular Aggregation. The structure of {Zn(S$_2$COEt)$_2$L}$_\infty$ (**1**) forms a one-dimensional supramolecular

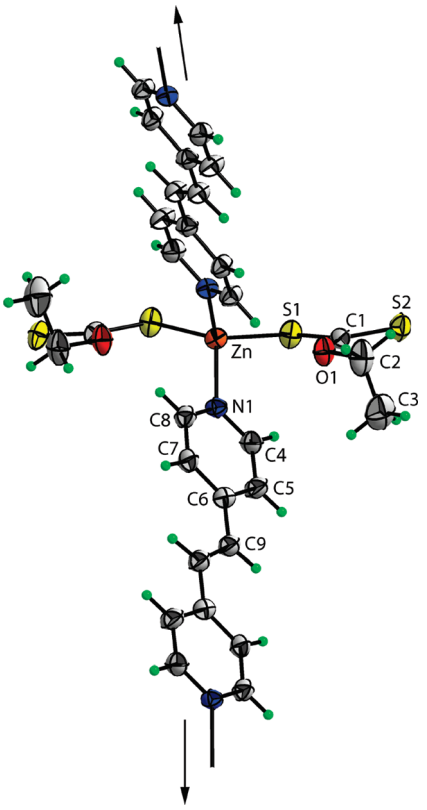

Figure 1. Portion of the polymeric structure of $\{Zn(S_2COEt)_2L\}_\infty$ (**1**) showing the crystallographic numbering scheme employed.

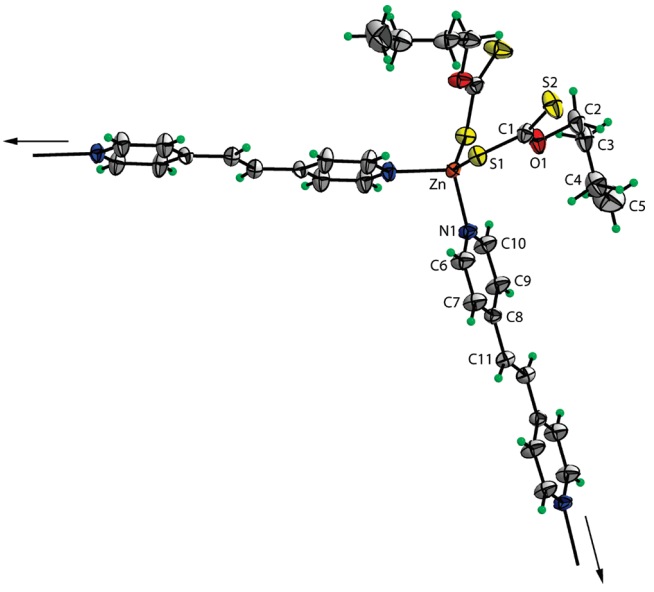

Figure 2. Portion of the polymeric structure of $\{Zn(S_2COBu)_2L\}_\infty$ (**2**) showing the crystallographic numbering scheme employed.

polymer in the solid state. This product was obtained from the slow evaporation of chloroform/acetonitrile (4/1) solutions containing products from the reaction of either 1:1 (to form a supramolecular polymer) or 2:1 (to form a bimetallic species) molar equivalents of $Zn(S_2COEt)_2$ and L. A portion of the polymer is shown in Figure 1 and key geometric parameters are collected in Table 2. The structure crystallizes in the monoclinic space group $C2/c$ and the asymmetric unit comprises $1/2\{Zn(S_2COEt)_2L\}$ in

Table 2. Selected Interatomic Parameters (Å, °) for 1 and 2[a]

parameter	1	2
Zn−S1	2.3146(7)	2.2998(5)
Zn−N1	2.056(2)	2.0613(17)
S1−C1	1.728(3)	1.729(2)
S2−C1	1.650(3)	1.650(2)
C1−O1	1.337(3)	1.331(3)
S1−Zn−N1	106.95(6)	106.08(5)
S1−Zn−S1^i	105.70(4)	130.45(3)
S1−Zn−N1^i	118.13(6)	104.29(5)
N1−Zn−N1^i	101.64(11)	102.64(10)
Zn−S1−C1	106.21(9)	100.05(7)

[a] Symmetry operation i: $-x, y, 1/2 - z$.

which the zinc atom lies on a 2-fold axis of symmetry and L is disposed about a center of inversion. The zinc atom exists in a distorted tetrahedral geometry defined by a N_2S_2 donor set. The xanthate ligands function in the monodentate mode, there being neither significant intra- nor intermolecular interaction between the zinc and S2 atoms. This feature of the structure is borne out by the systematic variation in the C−S distances, with that involving the zinc-bound S1 atom being longer than the other which has significant thione character, that is, 1.728(3) Å cf. 1.650(2) Å. Interestingly, the orientation of the xanthate ligands is such so as to place the oxygen atom in close proximity to zinc. The Zn···O1 separation of 3.062(3) Å is not considered to represent a significant bonding interaction, consistent with a review on such contacts.[5d] Nevertheless, the Zn···O1 contact may be responsible for some of the distortion from the ideal tetrahedral geometry. The range of angles subtended by the N_2S_2 donor set is 101.63(11) to 118.14(6)°, with the widest being opposite the O1 atom. Crystals of the *n*-butyl analogue (**2**) were also obtained from a chloroform/acetonitrile solution containing 2:1 mol equiv of $Zn(S_2COBu)_2$ and L. These were also found to be monoclinic with space group $C2/c$ but are not isomorphous with the ethylxanthate analogue **1**; see below. A portion of the polymeric structure, showing atom labeling, is shown in Figure 2.

The crystallographic symmetry found in the structure of **1** is also found in the structure of **2** and the coordination geometries are in essential agreement, but there are some interesting variations in geometric parameters worth highlighting, Table 2. The Zn−S bond distance in **2** is significantly shorter than in **1**, but the Zn−N distance follows the opposite trend. This is a likely consequence of the shorter intramolecular Zn···O1 interaction in **2** of 2.8842(16) Å. The tetrahedral angles subtended by the N_2S_2 donor set span a wider range in **2**, that is, 102.65(10) to 130.45(3)°, with the widest angle involving the S1 atoms, again be correlated with the close approach of the O1 atoms to zinc; Figure 2. This implies a different orientation of the xanthate ligands in **1** compared to that in **2** as discussed further below.

To a first approximation, both structures adopt a zigzag motif, each with a base vector along the [101] direction; see Figure 3. The pivot angles for each polymeric chain, as defined by the N−Zn−N angles, are almost identical, Table 2. The distance between the bridged zinc atoms in both structures is 13.5 Å, but the polymer repeat distance, measured as the Zn···Zn separation between successive dinuclear units of 22.2 Å in **2**, is longer than 19.3 Å found in **1**. At first this might seem an odd result given that the angle subtended at zinc by the nitrogen donors is effectively the same in both structures coupled with the equivalence of the N···N separations within the bridging entities.

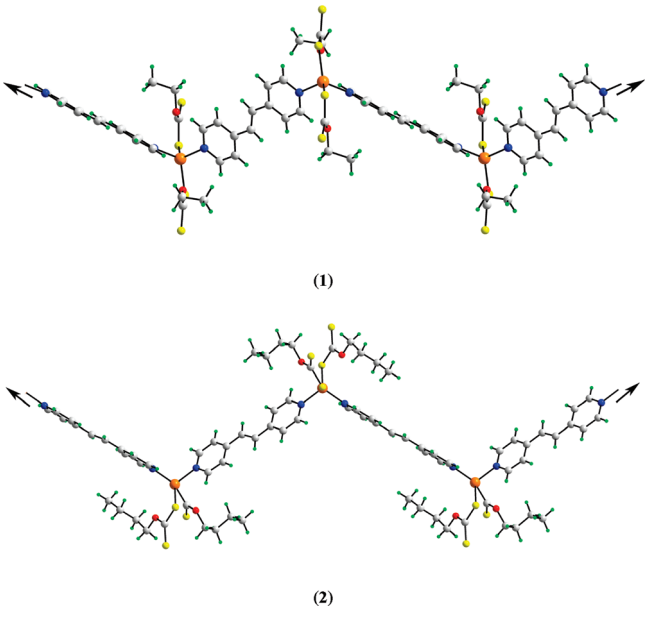

Figure 3. Polymeric strands in $\{Zn(S_2COEt)_2L\}_\infty$ (**1**) and $\{Zn(S_2COBu)_2L\}_\infty$ (**2**).

However, this feature of the structures is readily explained in terms of the relative disposition of the successive bridging ligands, conveniently quantified by the dihedral angles between pyridine residues bound to the same zinc atom: the greater the dihedral angle, the greater the twist, and the longer the Zn···Zn separation; the dihedral angles are 54.649(8)° for **1** cf. 82.72(4)° for **2**. Therefore, the polymeric strands in **2** are slightly more extended than found for **1**. The major difference between the polymeric chains is found in the relative orientation of the xanthate ligands. In the structure of **1**, the xanthate ligands are effectively coplanar so that the dihedral angle formed between the two S_2CO planes is 4.7(1)°. By contrast, the comparable angle in **2** is significantly greater at 39.6(1)°. As emphasized in Figure 3 and in the space filling diagrams (Figure S1 in the Supporting Information), the xanthate ligands at each zinc atom in **1** are directed to alternate sides of the polymer. In **2**, the xanthate ligands at each zinc atom are directed to one side of the polymer only, with alternate orientations at each junction of the polymer backbone. Globally, the crystal packing in **1** comprises layers of translationally related zig-zag chains (Figure S2a) with the xanthate ligands orientated above and below the layers allowing for their interdigitation with neighboring layers via C−H···S contacts (Figure S2b).[18a] A comparable crystal packing is found in **2**, but the translationally related supramolecular chains are spaced further apart as seen in the Zn···Zn separation between adjacent chains of 9.66 Å cf. 6.58 Å in **1** (Figure S2c). This observation is directly correlated with the different orientations of the xanthate ligands. The more open arrangement of the layers formed in **2** is compensated by closer interactions between the somewhat flattened layers connected by C−H···S contacts (Figure S2d).[18b]

A new structural motif is found in the third structure to be described, that is, $\{[Zn(S_2COCy)_2]_2L\}$ (**3**), characterized crystallographically as a dichloroform solvate, that is, **3.2CHCl$_3$**, which, by contrast to the previously described polymeric structures, is bimetallic, as shown in Figure 4; selected geometric parameters are listed in Table 3. Crystals of **3.2CHCl$_3$** were obtained under the same conditions as for

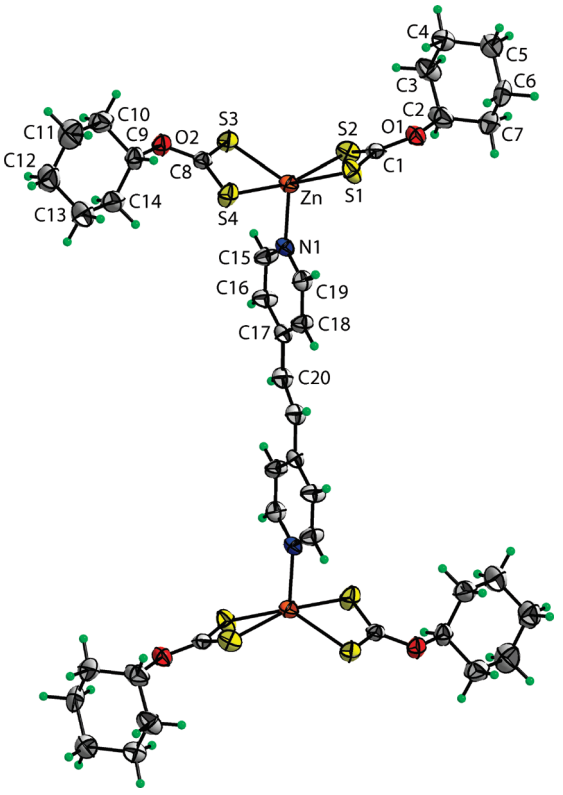

Figure 4. The dinuclear structure of centrosymmetric $\{[Zn(S_2COCy)_2]_2L\}\cdot 2CHCl_3$ (**3**) showing the crystallographic numbering scheme employed. Chloroform molecules of crystallization are omitted for clarity.

Table 3. Selected Interatomic Parameters (Å, °) for 3.2CHCl$_3$

parameter		parameter	
Zn−S1	2.3218(13)	Zn−S2	2.5894(15)
Zn−S3	2.3273(13)	Zn−S4	2.6586(14)
Zn−N1	2.044(3)	S1−C1	1.712(5)
S2−C1	1.683(4)	S3−C8	1.708(5)
S4−C8	1.683(4)	C1−O1	1.320(5)
C8−O2	1.328(5)	S1−Zn−S2	73.81(4)
S1−Zn−S3	134.55(5)	S1−Zn−S4	101.17(4)
S1−Zn−N1	112.68(10)	S2−Zn−S3	100.78(4)
S2−Zn−S4	165.30(4)	S2−Zn−N1	100.07(10)
S3−Zn−S4	72.58(4)	S3−Zn−N1	112.68(10)
S4−Zn−N1	94.61(10)	Zn−S1−C1	86.36(16)
Zn−S2−C1	78.62(17)	Zn−S3−C8	87.74(14)
Zn−S4−C8	77.87(16)		

1 and **2** and crystallize in the triclinic space group $P\bar{1}$ with $1/2\{[Zn(S_2COCy)_2]_2L\}$ and one chloroform molecule comprising the asymmetric unit. Immediately obvious in **3.2CHCl$_3$** is the increase in coordination number from four as in **1** and **2**, to five, with the zinc atom existing within a NS_4 donor set. This increase occurs as only one nitrogen atom coordinates to zinc allowing the xanthate ligand to function in the bidentate mode, albeit forming asymmetric Zn−S bond distances. The coordination geometry about the zinc atom is intermediate between trigonal bipyramidal, for which the weakly bound S2 and S4 donor atoms could be thought to define the axial positions, and square pyramidal, for which the N1 atom defines the apical position. The intermediate coordination geometry is emphasized by the value of $\tau = 0.51$, cf. $\tau = 0.0$ for an ideal square pyramid and $\tau = 1.0$ for an ideal trigonal bipyramid.[19] It should be mentioned here that the xanthate-bound R substituent does not exert a significant influence upon the electronic structure

of the ligand according to systematic crystallographic and theoretical studies into this question.[20] So, electronic effects cannot be cited as a reason for the difference coordination modes observed in **1**−**3.2CHCl$_3$**. As might be expected from the different structures, there are some systematic variations in geometric parameters are worth noting. The Zn−S bond distances in **3.2CHCl$_3$** are systematically longer than those in **1** and **2**, reflecting the increase in coordination number at zinc. This is further reflected in the reduced differences in the C−S bond distances in **3.2CHCl$_3$** compared with the situation for both **1** and **2**. Globally, molecules of **3** pack to form a two-dimensional grid as layers in the *ac*-plane comprising $[Zn(S_2COCy)_2]_2$ have L alternating on either side. The channels (ca. dimensions 8.5 × 13.8 Å) thus formed encapsulate the solvent molecules which are held in place via C−H···S interactions,[18c] the channels also contain cyclohexyl residues; see Figure S3.

In summary, regardless of the stoichiometric ratio of the $Zn(S_2COR)_2$ and L reactants, 1:1 adducts resulting in supramolecular zigzag chains are found when R = Et (**1**) and R = *n*-Bu (**2**). Conversely, only bimetallic aggregates are found when the steric bulk is increased, that is, R = Cy (**3**). These results show that steric control over supramolecular aggregation as a design principle in crystal engineering is extended to metal xanthates, which possess only one organic substituent compared with dithiocarbamates and dithiophosphates.[3,4] Given that two distinct motifs were found in the present study, it was thought of interest to determine their thermal decomposition and photophysical properties.

Thermal Decomposition. Thermogravimetric analyses of the polymeric species **1** and **2** showed a common decomposition pathway but one quite distinct to that observed for the bimetallic species **3**. For the polymeric species, decomposition occurs in two well-defined steps. The first step, with onset temperature = 112 °C for **1** and 120 °C for **2**, is consistent with the loss of the diimine ligand, L. The second step (onset 161 and 157 °C, respectively) terminates (673 and 485 °C, respectively) in the formation of ZnS in the form of sphalerite (JCPDS PDF 5-0566) consistent with previous reports on related zinc xanthate precursors.[3a,21] For pure **3**, that is, after drying to remove the solvent chloroform (see Experimental Procedures), decomposition occurs gradually (onset temperature 118 °C) and in one step only; sphalerite is again the final product (393 °C).

Diffuse Reflectance Spectra. The diffuse reflectance spectra are reproduced in the form of α/S via the Kubelka−Munk function:[22] $\alpha/S = (1 - R)^2/2R$ (where α is the absorption coefficient, S is the scattering coefficient, and R is the reflectance), as shown in Figure 5. The spectrum of the free ligand, L, can be resolved into two distinctive parts. The more intense high-energy band in the 200−380 nm region is attributed to a transition within the terminal pyridine residue and the low-energy part in the 380−550 nm region of low intensity due to the transitions of the conjugated π-system. The spectral features observed for $[ZnL]^{2+}$ replicates those of the free ligand, L, indicating only intraligand transitions of L are produced in the zinc compound. However, there are significant differences in the reflectance spectra between the homoleptic $Zn(S_2COR)_2$ compounds and those of **1** (being representative of **1** and **2**) and **3**. The reflectance spectra of the complexes can be classified to three bands in order of increasing energy, that is, A, B, and C. The A-absorption band with intermediate intensity, appearing in the 450−650 nm region, was observed in both **1** and **3**, while this band was very weak for the parent $Zn(S_2COCy)_2$ compound and appeared only as a trace for $Zn(S_2COEt)_2$; this low-energy band was not found for either $[ZnL]^{2+}$ or $K(S_2COR)$. These results suggested that the low-energy reflectance band might be associated with LMCT or interligand transfer.

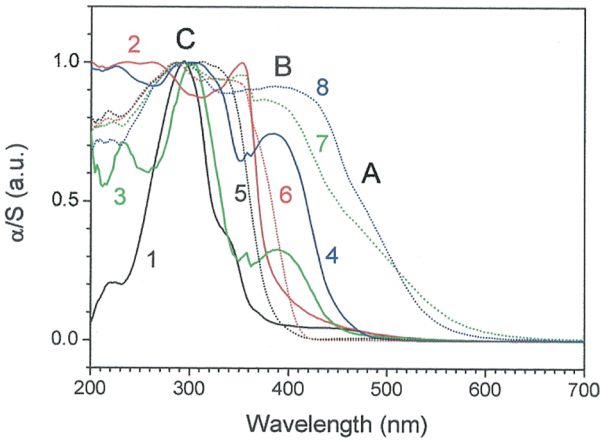

Figure 5. Diffuse reflectance spectra measured at room temperature in the solid-state: 1, L; 2, $[ZnL]^{2+}$; 3, $K(S_2COCy)$, 4, $K(S_2COEt)$; 5, $Zn(S_2COCy)_2$; 6, $Zn(S_2COEt)_2$; 7, $\{[Zn(S_2COCy)_2]_2L\}$ (**3**); and 8, $\{Zn(S_2COEt)_2L\}_\infty$ (**1**).

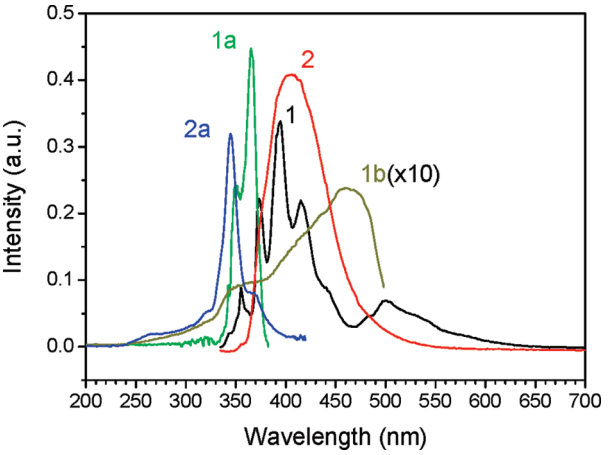

Figure 6. PL and excitation spectra of L and $[ZnL]^{2+}$ measured in the solid state at T = 10 K: L (1, λ_{exn} = 325 nm; 1a: λ_{ems} = 396 nm; 1b: λ_{ems} = 550 nm) and $[ZnL]^{2+}$ (2: λ_{exn} = 325 nm, 2a: λ_{ems} = 450 nm).

Luminescence. Prior to the characterization of the luminescence properties of **1** and **3**, the photoluminescence (PL) spectra of L, $[ZnL]^{2+}$, $K(S_2COCy)$, $K(S_2COEt)$, $Zn(S_2COCy)_2$, and $Zn(S_2COEt)_2$ were measured.

L and $[ZnL_2]^{2+}$. Figure 6 shows PL and excitation spectra of the free ligand L and $[ZnL]^{2+}$ measured in the solid state at T = 10 K. The PL spectrum of the free ligand L comprises sharp bands appearing in the 340−470 nm region, and a broadband in the 470−600 nm region. The sharp bands are vibronically distorted luminescence originating from the pyridine residue. The low-energy emission was quenched by coordination to zinc. This is unusual, since complexation of the π-conjugated chromophore should enhance the luminescence intensity owing to the increased rigidity in L resulting from complexation to zinc. The excitation spectra of the high-energy and the low-energy bands of L were different, as illustrated in Figure 6. The excitation spectra illustrated the mirror-images of their corresponding emission bands. These results suggested that the broad

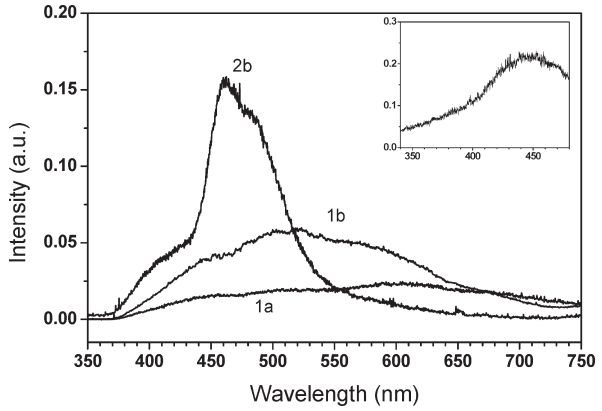

Figure 7. PL spectra of $Zn(S_2COCy)_2$ (1) and $K(S_2COCy)$ (2) measured in the solid state at $T = 10$ K (a) and RT (b). Inset: excitation spectrum of $Zn(S_2COCy)_2$ ($\lambda_{ems} = 600$ nm, $T = 10$ K).

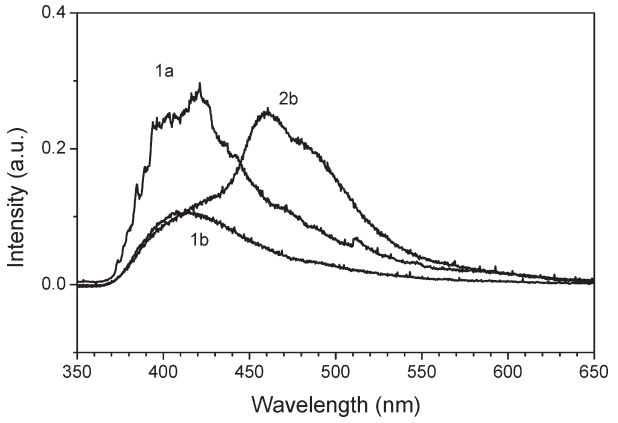

Figure 8. PL spectra of $[Zn(S_2COEt)_2]$ (1) and $K(S_2COEt)$ (2) measured in the solid state at $T = 10$ K (a) and RT (b).

low-energy band is due to the luminescence originating from the conjugated π-system.

$K(S_2COR)$ and $Zn(S_2COR)_2$. As shown in Figures 7 and 8, $K(S_2COR)$ produced similar PL spectra, independent of the nature of the R groups. The spectra comprise two main bands, peaking at 455 (R = Cy) and 460 (R = Et) nm, respectively, with a high-energy shoulder in the 360−430 nm region. The low-energy band is a typical intraligand luminescence originating from S atoms and the high-energy emission could be associated with the lone-pair electrons of O. By contrast, the spectral shapes of $Zn(S_2COR)_2$ were very affected by the nature of the *R* group. As shown in Figure 7, the spectral features observed for $Zn(S_2COCy)_2$ are quite distinct from those of $K(S_2COCy)$. At room temperature, $Zn(S_2COCy)_2$ produced very broad luminescence, ranging from 370 to 700 nm, with lower intensity than that of $K(S_2COCy)$. At 10 K, the intensity was reduced. The excitation spectrum (inset in Figure 7) corresponds to the A-reflectance band appearing as a trace. By contrast, $Zn(S_2COEt)_2$ produced only high-energy luminescence as the main band, which corresponds to the high-energy shoulder of the intraligand luminescence. At 10 K, the intensity of the high-energy luminescence was enhanced. These results indicated the observed luminescence of $Zn(S_2COCy)_2$ was associated with the charge transfer process between S and Zn and that of $Zn(S_2COEt)_2$ was associated with the intraligand transition of the xanthate ligand.

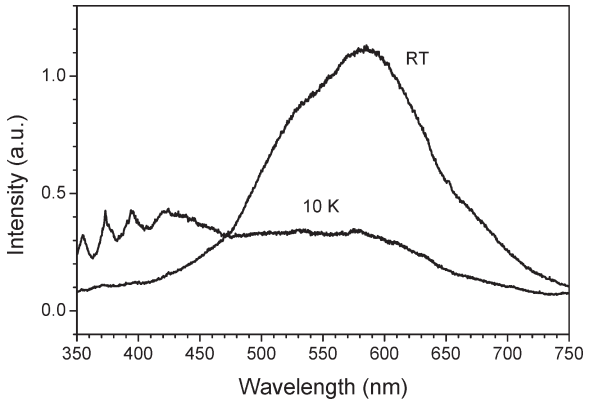

Figure 9. PL spectra of dinuclear $\{[Zn(S_2COCy)_2]_2L\}$ (**3**) measured in the solid state at $T = 10$ K and RT.

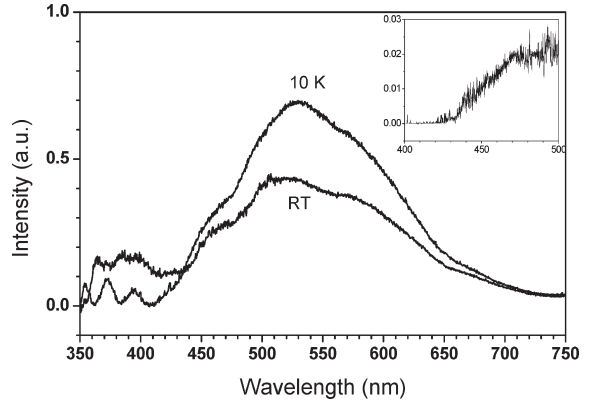

Figure 10. PL spectra of polymeric $\{Zn(S_2COEt)_2L\}_\infty$ (**1**) measured in the solid state at $T = 10$ K and RT. Inset: excitation ($\lambda_{ems} = 600$ nm) spectrum ($T = 10$ K).

$\{[Zn(S_2COCy)_2]_2L\}$ and $\{Zn(S_2COEt)_2L\}_\infty$. At room temperature, dinuclear $\{[Zn(S_2COCy)_2]L\}_2$ (**3**) produced orange luminescence, as shown in Figure 9. Compared with $Zn(S_2COCy)_2$, the luminescence intensity of (**3**) was markedly enhanced (more than 20 times at room temperature) and the peak position was red-shifted to 580 nm. At $T = 10$ K, the intensity of the 580 nm luminescence was reduced, and multiple lines, corresponding to the intraligand emission from the pyridine ring of L, appeared in the 350−450 nm region. For polymeric $\{Zn(S_2COEt)_2L\}_\infty$ (**1**), the PL spectral shape was similar to that of (**3**), Figure 10, but the peak position was blue-shifted. At low temperature, the intensity of the yellow luminescence was enhanced. For **1**, the excitation spectrum of the 600 nm emission measured at $T = 10$ K, inset in Figure 10, reflected the mirror image of the PL band, indicating that the A-band excited states were responsible for the emitting centers. The intraligand luminescence of L appeared in the UV region as a trace at low temperature. In summary, **3**, with the five-coordinate NS_4 geometry, produced markedly enhanced luminescence in the visible region, compared with polymeric **1** with a tetrahedral N_2S_2 geometry.

CIS post-HF Calculations and Assignment of Transitions. Quantum mechanical calculations were performed on $Zn(S_2COCy)_2$ and **3** to elucidate the ordering of the excited states and the electronic transitions using the Gaussian 03 program.[23] Initially, each molecular geometry was optimized with SDD basis functions (LanL2DZ for Zn; 6-31G(d) for S, 6-31G for C bonded to S and N, and LanL2MB for the

Table 4. Some HF Molecular Orbitals Calculated for {[Zn(S_2COCy)$_2$]$_2$L} (3)

MO	hartree	2Zn				4S_2COCy							L	
						8S				4O	4C		8C	2N
		s	p_x	p_y	p_z	*s*	p_x	p_y	p_z	p_y	s	p_y	p_z	p_z
*l*11	0.17	43		3			3		26		21	2		
*l*10	0.17	43		3			3		26		21	2		
*l*9	0.17		14		52	21		5		2		6		
*l*8	0.16		54		1	18	3	3				11	7	
*l*7	0.16		26		45	27			1					
*l*6	0.15		19		46	27								4
*l*5	0.15		39		20	21				6		13		
*l*4	0.15		20		43	23						8		
*l*3	0.14	6		47						14		27		
*l*2	0.14	6		47						14		27		
*l*1	0.09				13	5							67	14
*h*1	−0.29						42		58					
*h*2	−0.29						42		58					
*h*3	−0.30							100						
*h*4	−0.30							100						
*h*5	−0.31							100						
*h*6	−0.31							100						
*h*7	−0.31						47		38				15	
*h*8	−0.32						58		42					
*h*9	−0.32								13					87
*h*10	−0.34							54	10	36				
*h*11	−0.34							45	20	35				
*h*12	−0.35							66		33				
*h*13	−0.35							66		33			-	
*h*14	−0.35												100	
*h*15	−0.35												100	

remaining atoms) and then a CIS calculation was performed with the ZINDO semiempirical method. As the crystal structure of Zn(S_2COCy)$_2$ is not available to provide a starting model, the structure was assumed to be mononuclear with zinc within a distorted tetrahedral S_4 donor set, an assumption based on literature precedents for related zinc 1,1-dithiolate molecules with bulky substituents.[3b]

{[Zn(S_2COCy)$_2$]$_2$L}. Comparison of key geometric parameters determined from the experimental (X-ray) and optimized structures are listed in Table S1 (Supporting Information), showing a high degree of concordance. The calculated HF orbitals are listed in Table 4; for ease of comparison, the following discussion pertains to one Zn center only. The combination of the p_x and p_z orbitals of each S atom gives rise to the highest occupied molecular orbitals (HOMOs), doubly degenerate *h*1 and *h*2, in which the contribution of the p_z orbital is 58%; here, the molecular axis is taken as the *y*-axis. The combination of the remaining p_y orbitals of four S atoms defines the next four HOMOs, *h*3 − *h*6. The *h*7 and *h*8 HOMOs also result from the combination of the S atoms' p_x and p_z orbitals. For these HOMOs, the contribution of the p_x orbital is greater than the p_z orbital. A minor contribution to *h*7 is made by the p_z orbitals of C atoms in L. The *h*9 orbital has some p_z character from S and a major contribution (87%) from p_z of the N atoms of L. The next four *h*10 − *h*13 orbitals have significant p_y character of S along with O p_y character. The doubly degenerate *h*14 and *h*15 orbitals correspond to the π orbitals of the C of L. The first lowest unoccupied molecular orbital (LUMO), *l*1, primarily corresponds to the π^* orbital of L along with some character of the Zn atom's p_z orbital. The doubly degenerate *l*2 and *l*3 LUMOs comprise significant Zn p_y character with minor contributions from the p_y orbitals of C and O within the xanthate ligand. The next six *l*4 − *l*9 LUMOs are formed by the linear combination of the Zn atom p_x and p_y orbitals as the main contributions with smaller contributions from the S atoms' *s* orbitals. Finally, the high-energy *l*10 and *l*11 LUMOs are formed from major contributions from the Zn *s* orbital along with contributions from the S p_z orbitals and *s* orbitals of the xanthate C atoms.

The results for some low-lying excited states and the oscillator strengths are listed in Table S2. According to the energy gap and the oscillator strength considerations, the listed excited states can be classified to three groups: 1B − 2B, 3B − 8B, and 9B − 14B. These three groups are assigned as being responsible for the A-, B-, and C-reflectance bands, respectively, as indicated in Figure 5. In the group A, the first excited state, 1B, arose from the *h*2 → *l*3 and *h*1 → *l*2 transitions. The contributions of Zn to the upper levels are greater than those by the O and C atoms. The transition mechanisms of the 1A, 2A, and 2B excited states are similar to that of the 1B excited state. However, the calculated oscillator strengths of the transition from the *X* ground state to the A-band excited states were small or even zero. The A-reflectance band appeared as a low-energy shoulder and is assigned to transitions to the excited states of the group A, which are charge transfer in nature. Several excited states were involved in the B-band transition. Among the calculated transitions, the transition from the X ground state to the 4B excited state is the largest with $f = 1.67$; transitions to the 3B and 5B excited states are also large with $f = 0.463$ and 0.318, respectively. The 4B excited state predominantly arises from the *h*9 → *l*1 transition, indicating that this is strongly associated with the intraligand transition of L. The 3B excited state arose from the *h*4 → *l*3 and *h*3 → *l*2 transitions, and the 5B state from *h*6 → *l*3 and *h*5 → *l*2 transitions. These transitions are associated with the charge transfer from S to Zn with an additional but smaller contribution from an intraligand transition in the xanthate ligand. In group C, the transition from the X ground state to the 12A excited state is the second largest among all calculated transitions with $f = 1.14$, Table S2, and is due

to the $h10 \rightarrow l2$ and $h11 \rightarrow l3$ transitions. According to the atomic charges determined from the Mulliken population analysis, for the X → 12A transition, the changes of the atomic charges of Zn, and the xanthate- S, C, and O atoms are +0.98, −0.45, +0.21, and −0.21 per atom, respectively. This indicates that the X → 12A transition was associated primarily with electronic transitions of the lone-pair electrons of S to Zn along with a minor contribution of the intraligand transition of the xanthate ligand. The electron density isocontours responsible for the strong X → 12A transition of $\{[Zn(S_2COCy)_2]_2L\}$ are shown in Figure 11. The 12B excited state with $f = 0.233$ results from the $h14 \rightarrow l1$ transition which corresponds to the $\pi \rightarrow \pi^*$ transition of L.

For **3**, the charge transfer process clearly plays a key role in the observed visible luminescence. The high-energy excitation ($\lambda_{exn} = 325$ nm) predominantly induced the charge transfer from S to Zn, followed by the nonradiative energy transfer from the upper C excited states to the lower A excited states, with subsequent radiative transition from the A excited states to the ground state.

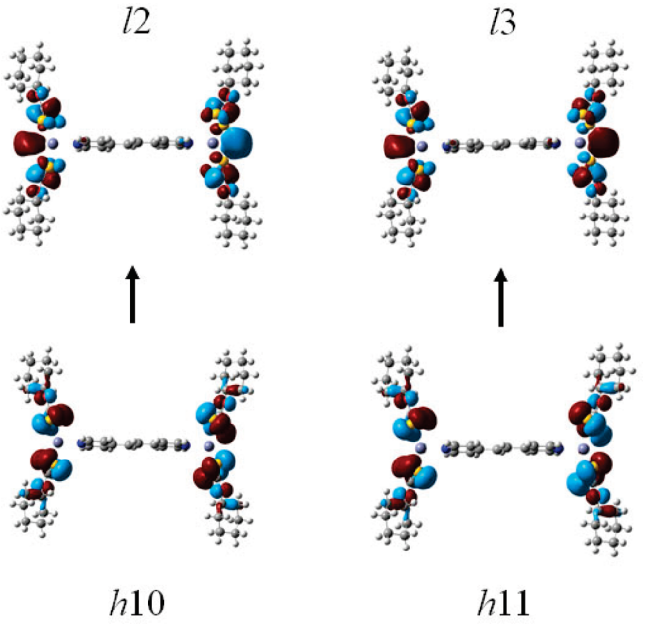

Figure 11. Electron density isocontours of $\{[Zn(S_2COCy)_2]_2L\}$ (**3**) responsible for the strong charge transfer transitions from S to Zn.

$Zn(S_2COCy)_2$. As listed in Table 5, the first four HOMOs ($h1 - h4$) resulted from the linear combination of the p_x, p_y, and/or p_z orbitals of S, and the next two HOMOs ($h5$ and $h6$) were contributed from the p orbitals of S and O atoms. For the $l1 - l6$ LUMOs, the p orbitals of Zn are main components, with contributions of at least 49%, and the s and p orbitals of S are minor components with the contribution of less than 25%. Some excited states are listed in Table S3. According to the energy gaps, the 1B − 1A, 2B − 5A, and 6B − 9B excited states are responsible for the A-, B-, and C-reflectance bands, respectively.

For the group A, the two excited states arose from the transitions from the $h2$ and $h3$ HOMOs to the $l1$ and $l2$ LUMOs. The calculated oscillator strength revealed that these transitions were forbidden. Experimentally, the A-reflectance band was not observed, as indicated in Figure 5. For the group B transitions, most are weak, in which the $h1 - h3$ HOMOS and the $l1 - l3$ LUMOs were involved as the low and the upper levels, respectively. The change in the Zn charge was as much as +0.3 per atom, indicating that the charge transfer from S to Zn was a main component. However, the calculated oscillator strengths of these transitions are less than 0.1, and accordingly, the B-band transition was observed only as a weak band.

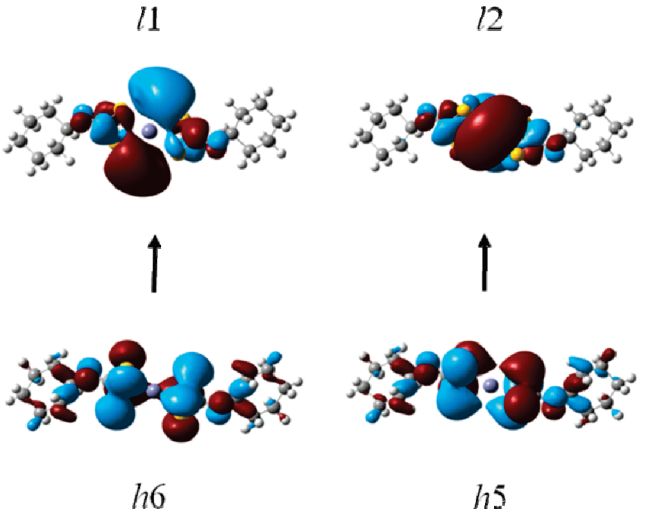

Figure 12. Electron density isocontours for the $Zn(S_2COCy)_2$ molecule responsible for the strong C-band transition.

Table 5. Some HF Molecular Orbitals Calculated for $Zn(S_2COCy)_2$

MO	hartree	Zn				2S$_2$COCy												
						4S				2O			2C				2Cy		
		s	p_x	p_y	p_z	*s*	p_x	p_y	p_z	p_x	p_y	p_z	*s*	p_x	p_y	p_z	p_x	p_y	p_z
*l*7	0.20		3	14			8	9	7				34	1	3				
*l*6	0.15		41	8		12	5	1	10	3		3		8	3	4			
*l*5	0.15		41	8			5	2	10	2	1	5		4		12			
*l*4	0.14		20	50		24							5						
*l*3	0.14	4	57			5	5	19					7						
*l*2	0.11				59	15								9	4	5			
*l*1	0.11		34	26		15				3		5		4		12			
*h*1	−0.32						56		44										
*h*2	−0.33						3	50	47										
*h*3	−0.33						28	55	17										
*h*4	−0.33						55		45										
*h*5	−0.37						5	4	53	18	5	15							
*h*6	−0.37						35	9	17	14	5	20							
*h*7	−0.39			4	9		17	58	6		6								
*h*8	−0.43						5	7		6	8					3	29	26	

In group C, the oscillator strength of the X → 6B transition is the largest with $f = 0.676$. The 6B excited state arose from the $h6 \rightarrow l1$ and $h5 \rightarrow l2$ transitions as shown in Figure 12. However, the change of the charge of Zn for this transition is only 0.13. It is suggested that the charge transfer process competed with the intraligand transition of xanthate. In the C group, the largest change of the electron charge of Zn was found in the X → 8B transition with +0.61, for which the calculated oscillator strength of $f = 0.098$ is intermediate. Thus, the C-band excitation can be assigned mainly as being due to the intraligand transition of xanthate with a contribution by the charge transfer from S to Zn.

From theory for the binary zinc xanthate compounds, two optical processes were responsible for the observed luminescence: the charge transfer process from S to Zn and the intraligand process. For $Zn(S_2COCy)_2$, the charge transfer process took place more preferentially than the intraligand process, while for $Zn(S_2COEt)_2$, the opposite was observed.

Conclusions

The steric profile of the xanthate ligands in $Zn(S_2COR)_2$ proved pivotal in determining the dimensionality of supramolecular aggregates formed between $Zn(S_2COR)_2$ and *trans*-1,2-bis(4-pyridyl)ethylene (L). Thus, for bulky R = Cy, a zero-dimensional dinuclear species was formed, that is, $\{[Zn(S_2COCy)_2]_2L\}$, with chelating xanthate ligands leading to a five-coordinate NS_4 geometry. Reducing the steric bulk to R = Et and *n*-Bu, allowed for the formation of one-dimensional polymeric chains with N_2S_2 tetrahedral zinc as the xanthate ligands are now monodentate. The different supramolecular motifs result in different coordination geometries, and these are shown to influence the observed photophysical properties. The A-band excited states are responsible for the observed luminescence of the dinuclear $\{[Zn(S_2COCy)_2]_2L\}$ and the polymeric $\{Zn(S_2COEt)_2L\}_\infty$ structures. The CIS HF results indicate that the A-band excited states arises from the transitions from two p_x and p_z orbitals of S to the p_y orbital of Zn in the main, with the intraligand transition of xanthate having a smaller contribution. For $\{Zn(S_2COEt)_2L\}_\infty$ the A-band luminescence was significantly weaker than $\{[Zn(S_2COCy)_2]_2L\}$, a result directly correlated with the reduced formal coordination number in the polymeric species.

Acknowledgment. The University of Singapore (NUS) is thanked for a research grant (R-143-000-151-112) to E.R.T.T. Leng Lee Eng (TGA) and Toh Soh Lian (XRD), both of NUS, are thanked for assistance. J-G.K. and Y.-K.J. acknowledge fellowships awarded by the BK 21 program.

Supporting Information Available: Crystallographic information files for the structures reported herein, crystal packing diagrams (Figures S1−S3), comparison of geometric parameters from optimization calculations (Table S1), and details of CI excited states (Tables S2−S3). This material is available free of charge via the Internet at http://pubs.acs.org.

References

(1) (a) Wang, S. N. *Coord. Chem. Rev.* **2001**, *215*, 79–98. (b) Erxleben, A. *Coord. Chem. Rev.* **2003**, *246*, 203–228. (c) Zheng, S. L.; Chen, X. M. *Aust. J. Chem.* **2004**, *57*, 703–712. (d) A. Barbieri, A.; Accorsi, G.; Armaroli, N. *Chem. Commun.* **2008**, 2185–2193.

(2) (a) Zhai, Q.-G.; Lu, C.-Z.; Wu, X.-Y.; Batten, S. R. *Cryst. Growth Des.* **2007**, *7*, 2332–2342. (b) Amiri, M. G.; Mahmoudi, G.; Morsali, A.; Hunter, A. D.; Zeller, M. *CrystEngComm* **2007**, *9*, 686–697. (c) Bao, Z.; Ng, K.-Y.; Yam, V. W.-W.; Ko, C.-C.; Zhu, N.; Wu, L. *Inorg. Chem.* **2008**, *47*, 8912–8920. (d) Jiang, T.; Zhang, X. M. *Cryst. Growth Des.* **2008**, *8*, 3077–3083. (e) Liu, Y.-Y.; Ma, J.-F.; Yang, J.; Ma, J.-C.; Su, Z.-M. *CrystEngComm* **2008**, *10*, 894–904. (f) Kuo, K.-L.; Huang, C.-C.; Lin, Y.-C. *Dalton Trans* **2008**, 3889–3898. (g) Wang, J.; Lin, Z. J.; Ou, Y.-C.; Yang, N.-L.; Zhang, Y.-H.; Tong, M. L. *Inorg. Chem.* **2008**, *47*, 190–199. (h) Habib, H. A.; Hoffmann, A.; Hoppe, H. A.; Steinfeld, G.; Janiak, C. *Inorg. Chem.* **2009**, *48*, 2166–2180. (i) Ren, H.; Song, T.-Y.; Xu, J.-N.; Jing, S.-B.; Yu, Y.; Zhang, P.; Zhang, L.-R. *Cryst. Growth Des.* **2009**, *9*, 105–112. (j) Cao, X.-Y.; Yao, Y.-G.; Batten, S. R.; Ma, E.; Qin, Y.-Y.; Zhang, J.; Zhang, R.-B.; Cheng, J.-K. *CrystEngComm* **2009**, *11*, 1030–1036. (k) Tong, X.-L.; Wang, D.-Z.; Hu, T.-L.; Song, W.-C.; Tao, Y.; Bu, Z.-H. *Cryst. Growth Des.* **2009**, *9*, 2280–2286.

(3) (a) Lai, C. S.; Lian, Y. X.; Yap, T. C.; Tiekink, E. R. T. *CrystEngComm* **2002**, *4*, 596–600. (b) Tiekink, E. R. T. *CrystEngComm* **2003**, *5*, 101–113. (c) Lai, C. S.; Liu, S.; Tiekink, E. R. T. *CrystEngComm* **2004**, *6*, 221–226. (d) Lai, C. S.; Tiekink, E. R. T. *CrystEngComm* **2004**, *6*, 593–605. (e) Chen, D.; Lai, C. S.; Tiekink, E. R. T. *CrystEngComm* **2006**, *8*, 51–58. (f) Tiekink, E. R. T. *CrystEngComm* **2006**, *8*, 104–118. (g) Benson, R. E.; Ellis, C. A.; Lewis, C. E.; Tiekink, E. R. T. *CrystEngComm* **2007**, 930–941.

(4) (a) Liu, Y.; Tiekink, E. R. T. *CrystEngComm* **2005**, *7*, 20–27. (b) Lai, C. S.; Tiekink, E. R. T. *Z. Kristallogr.* **2007**, *222*, 532–538. (c) Tiekink, E. R. T. *Appl. Organomet. Chem.* **2008**, *22*, 533–550.

(5) (a) Soh, S. F.; Lai, C. S.; Tiekink, E. R. T. *Acta Crystallogr.* **2002**, *E58*, m641–m643. (b) Klevtsova, R. F.; Leonova, T. G.; Glinskaya, L. A.; Larionov, S. V. *Russ. J. Coord. Chem.* **2000**, *26*, 172–177. (c) Larionov, S. V.; Glinskaya, L. A.; Leonova, T. G.; Klevtsova, R. F. *Koord. Khim.* **1998**, *24*, 909−914 (in Russian); (d) Tiekink, E. R. T.; Haiduc, I. *Prog. Inorg. Chem.* **2005**, *54*, 127–319.

(6) De la Durantaye, L.; McCormick, T.; Liu, X.-Y.; Wang, S.-N. *Dalton Trans.* **2006**, 5675–5682.

(7) Ho, K.-Y.; Yu, W.-Y.; Cheung, K.-K.; Che, C.-M. *Dalton Trans.* **1999**, 1581–1586.

(8) Xu, X.-J.; Liao, Y.; Yu, G.; You, H.; Di, C.-G.; Su, Z.-M.; Ma, D.-G.; Wang, Q.; Li, S.-Y.; Wang, S.-Q.; Ye, J.-P.; Liu, Y.-Q. *Chem. Mater.* **2007**, *19*, 1740–1748.

(9) Sun, R.; Li, Y.-Z.; Bai, J.; Pan, Y. *Cryst. Growth Des.* **2007**, *7*, 890–894.

(10) Sang, R.-L.; Xu, L. *Inorg. Chem.* **2005**, *44*, 3731–3737.

(11) Yu, T.-Z.; Zhang, K.; Zhao, Y.-L.; Yang, C.-H.; Zhang, H.; Qian, L.; Fan, D.-W.; Dong, W.-K.; Chen, L.-L.; Qiu, Y.-Q. *Inorg. Chim. Acta* **2008**, *361*, 233–240.

(12) (a) Truesdell, K. A.; Crosby, G. A. *J. Am. Chem. Soc.* **1985**, *107*, 1788–1789. (b) Highland, R. G.; Brummer, J. G.; Crosby, G. A. *J. Phys. Chem.* **1986**, *90*, 1593–1598. (c) Jordan, K. J.; Wacholtz, W. F.; Crosby, G. A. *Inorg. Chem.* **1991**, *30*, 4588–4593.

(13) Ngan, T.-W.; Ko, C.-C.; Zhu, N.-Y.; Yam, V. W.-W. *Inorg. Chem.* **2007**, *46*, 1144–1152.

(14) Yun, S.-S.; Kim, J.-K.; Jung, J.-S.; Park, C.; Kang, J.-G.; Smyth, D. R.; Tiekink, E. R. T. *Cryst. Growth Des.* **2006**, *6*, 899–909.

(15) 10. Kang, J.-G.; Cho, H.-K.; Park, C.; Yun, S.-S.; Kim, J.-K.; Broker, G. A.; Smyth, D. R.; Tiekink, E. R. T. *Inorg. Chem.* **2007**, *46*, 8228−8237.

(16) Cox, M. J.; Tiekink, E. R. T. *Z. Kristallogr.* **1999**, *214*, 184–190.

(17) (a) *SAINT. Version V5.6*; Bruker AXS Inc.: Madison, WI, 2000; (b) Sheldrick, G. M. *SADABS*; University of Gottingen: Germany, **2000**;(c) Beurskens, P. T.; Admiraal, G.; Beurskens, G.; Bosman, W. P.; García-Granda, S.; Smits, J. M. M.; Smykalla, C. The DIRDIF program system, *Technical Report of the Crystallography, Laboratory*; University of Nijmegen: Nijmegen, The Netherlands, 1992; (d) Sheldrick, G. M. *Acta Crystallogr.* **2008**, *A64*, 112–122. (e) *DIAMOND, Visual Crystal Structure Information System, Version 2.1e*; CRYSTAL IMPACT: Bonn, Germany, **2002**.

(18) Intermolecular interactions. In **1**: C5−H5···S2^{i} = 2.83 Å, C5···S2^{i} = 3.733(3) Å with angle at H5 = 159° for symmetry operation *i*: $-1/2 - x, 1/2 + y, 1/2 - z$. In **2**: C11−H11···S1^{i} = 2.88 Å, C11···S1^{i} = 3.591(2) Å with angle at H11 = 132° for symmetry operation *i*: $-x, -y, -z$; and C9−H9···S2^{ii} = 2.90 Å, C9···S2^{ii} = 3.782(2) Å with angle at H9 = 155° for symmetry operation *ii*: $-1/2 + x, -1/2 + y, z$. In **3.2CHCl$_3$**: C21−H21···S1^{i} = 2.77 Å, C21···S1^{i} = 3.580(5) Å with angle at H21 = 139° for symmetry operation *i*: $1 - x, 1 - y, 1 - z$.

(19) Addison, A. W.; Rao, T. N.; Reedijk, J.; van Rijn, J.; Verschoor, G. C. *J. Chem. Soc., Dalton Trans.* **1984**, 1349–1356.

(20) Buntine, M. A.; Cox, M. J.; Lim, Y. X.; Yap, T. C.; Tiekink, E. R. T. *Z. Kristallogr.* **2003**, *218*, 56–61.

(21) (a) Kosareva, L.; Larionov, S. V. *Izv. Sib. Otd. Akad. Nauk SSSR, Ser. Khim. Nauk* **1988**, *3*, 46–50. (b) Larionov, S. V. *Russ. J. Inorg. Chem.* **2001**, *46*, S66–S85.

(22) Kortüm, G. *Reflectance Spectroscopy*; Springer-Verlag: New York, 1969.

(23) Frisch, M. J.; Trucks, G. W.; Schlegel, H. B.; Scuseria, G. E.; Robb, M. A.; Cheeseman, J. R.; Montgomery Jr., J. A.; Vreven, T.; Kudin, K. N.; Burant, J. C.; Millam, J. M.; Iyengar, S. S.; Tomasi, J.; Barone, V.; Mennucci, B.; Cossi, M.; Scalmani, G.; Rega, N.; Petersson, G. A.; Nakatsuji, H.; Hada, M.; Ehara, M.; Toyota, K.; Fukuda, R.; Hasegawa, J.; Ishida, M.; Nakajima, T.; Honda, Y.; Kitao, O. ; Nakai, H.; Klene, M.; Li, X.; Knox, J. E.; Hratchian, H. P.; Cross, J. B.; Bakken, V.; Adamo, C.; Jaramillo, J.; Gomperts, R.; Stratmann, R. E.; Yazyev, O.; Austin, A. J.; Cammi, R.; Pomelli, C.; Ochterski, J. W.; Ayala, P. Y.; Morokuma, K.; Voth, G. A.; Salvador, P.; Dannenberg, J. J.; Zakrzewski, V. G.; Dapprich, S.; Daniels, A. D.; Strain, M. C.; Farkas, O.; Malick, D. K.; Rabuck, A. D.; Raghavachari, K.; Foresman, J. B.; Ortiz, J. V.; Cui, Q.; Baboul, A. G.; Clifford, S.; Cioslowski, J.; Stefanov, B. B.; Liu, G.; Liashenko, A.; Piskorz, P.; Komaromi, I.; Martin, R. L.; Fox, D. J.; Keith, T.; Al-Laham, M. A.; Peng, C. Y.; Nanayakkara, A.; Challacombe, M.; Gill, P. M. W.; Johnson, B.; Chen, W.; Wong, M. W.; Gonzalez C.; Pople, J. A. Gaussian 03, Revision C.02; Gaussian, Inc.: Wallingford, CT, 2004.